Polyhedron 29 (2010) 84–93

Contents lists available at ScienceDirect

Polyhedron

journal homepage: www.elsevier.com/locate/poly

Spin-state splittings of iron(II) complexes with trispyrazolyl ligands

Mireia Güell [a], Miquel Solà [a], Marcel Swart [a,b,*]

[a] Institut de Química Computacional and Departament de Química, Universitat de Girona, Campus Montilivi, 17071 Girona, Spain
[b] Institució Catalana de Recerca i Estudis Avançats (ICREA), 08010 Barcelona, Spain

ARTICLE INFO

Article history:
Available online 8 June 2009

Keywords:
Iron complexes
Pyrazolylborate ligands
Pyrazolylmethane ligands
Density Functional Theory

ABSTRACT

We report a computational study at the OPBE/TZP level on the chemical bonding and spin ground-states of mono-nuclear iron(II) complexes with trispyrazolylborate and trispyrazolylmethane ligands. We are in particular interested in how substitution patterns on the pyrazolyl-rings influence the spin-state splittings, and how they can be rationalized in terms of electronic and steric effects. One of the main observations of this study is the large similarity of the covalent metal–ligand interactions for both the borate and methane ligands. Furthermore, we find that the spin-state preference of an individual transition-metal (TM) complex does not always concur with that of an ensemble of TM-complexes in the solid-state. Finally, although the presence of methyl groups at the 3-position of the pyrazolyl groups leads to ligand–ligand repulsion, it is actually the loss of metal–ligand bonding interactions that is mainly responsible for shifts in spin-state preferences.

1. Introduction

In 1966, a versatile new class of ligands appeared, which combines some features of the cyclopentadienyl (Cp) and betadiketonate ligands [1]. These new complexes are the polypyrazolylborate anions with the general structure $[R_nB(pz)_{4-n}]^-$, where n can be 0, 1 or 2, pz is a pyrazol-1-yl group and R usually is H, an alkyl or aryl group (see Scheme 1). With $n = 1$ and R = H, this gives a tridentate ligand $[HB(pz)_3]^-$, which had been given the abbreviation Tp (for tripyrazolyl) and its substituents are then often denoted by superscripts (e.g. Tp^{3Me} for the 3-methyl analogue) [2].

Since the systematic name poly(pyrazol-1-yl)borates does not convey the mode of coordination of these ligands, these ligands are also called *scorpionates* [2] to provide an idea of how the ligand binds to metal ions. In almost all cases there are (at least) two pyrazolyl groups coordinated to the metal ion (see Scheme 2) and the resulting six-membered ring is in a deep boat form that brings the third group arching over the metal ion, like the tail of a scorpion. In the case of homoscorpionates this third group consists of a third pyrazolyl group, but it may also be formed by other groups (e.g. H, OR, SR, NR_2), i.e. the heteroscorpionates. However, the coordination of the metal with a third ligating group is not mandatory, since the Tp ligand can sometimes be only bidentate, as in complexes of Rh(I) and Pd(II) [3].

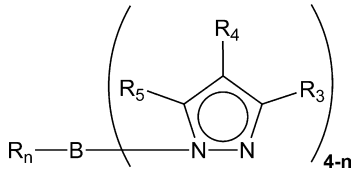

Scheme 1. General structure of $[R_nB(pz)_{4-n}]^-$, where n can be 0, 1 or 2, pz is a pyrazol-1-yl group and R can be H, an alkyl or aryl group.

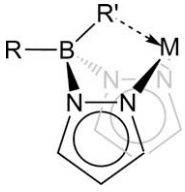

Scheme 2. Bonding in a polypyrazolylborate–metal complex.

Several transition-metal complexes have been observed where a metal is ligated by two of these Tp^x ligands (di-scorpionates, see Fig. 1) with an octahedral (homoleptic) metal coordination. In case of Fe(II), many of these have been classified as spin-crossover complexes (see Table 1), which are interesting complexes for technology and medicine, as they are able to switch between different states depending on the temperature, pressure, etc. However, not all of the di-scorpionate complexes show spin-crossover behavior, as is for instance the case for $Fe(Tp^{3,4,5\text{-}Me3})_2$ that remains

* Corresponding author. Address: Institut de Química Computacional and Departament de Química, Universitat de Girona, Campus Montilivi, 17071 Girona, Spain. Tel.: +34 972 183240; fax: +34 972 183241.
E-mail addresses: marcel.swart@icrea.es, marcel.swart@udg.edu (M. Swart).

0277-5387/$ - see front matter © 2009 Elsevier Ltd. All rights reserved.
doi:10.1016/j.poly.2009.06.006

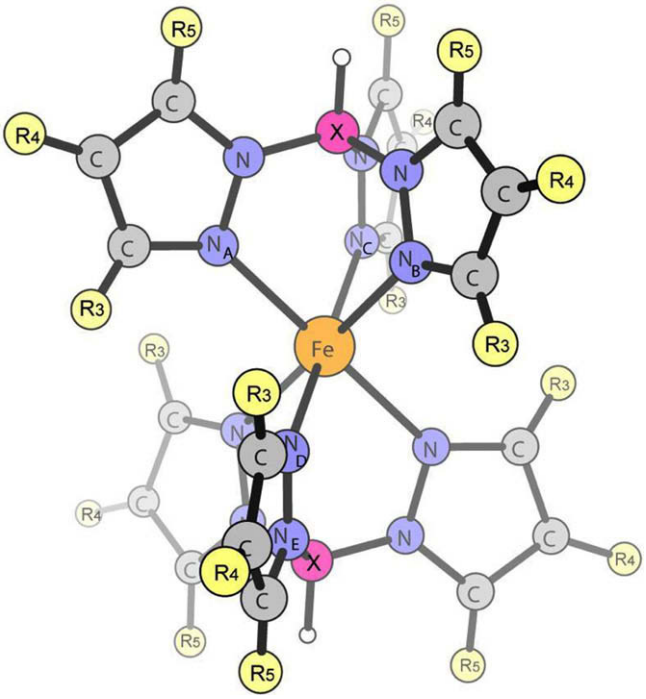

Fig. 1. Three dimensional representation of the Fe(II)-trispyrazolylborates T_b^x (X = B) and Fe(II)-trispyrazolylmethanes T_c^x (X = C).

high-spin even at low temperatures, or the parent complex $Fe(Tp)_2$ that remains low-spin up until ca. 420 K.

The reason for this different behavior is often attributed to steric intra-molecular interligand interactions between the 3-methyl groups, but electronic substituent effects can not be disregarded altogether and may even play a decisive role. Moreover, spin-crossover properties are generally believed to result from cooperative properties of a large number of these "molecules" within the solid phase, and which involve long-range intermolecular interactions, even though spin-crossover (SCO) has also been observed with complexes in solution [4–6]. Therefore, the origin for the differences in the spin-crossover behavior that are observed for different substituted di-scorpionate complexes (if any) remains unknown.

In principle, computational studies should be able to clarify (some parts of) this complex situation, as one could perform separate studies on the isolated complexes, and on the solid phase. By comparing these results, one could obtain detailed information about the parameters that govern the spin-crossover (SCO) phenomenon. However, there are a number of pitfalls that hamper this straightforward application of theory. The most important one regards the correct description of relative spin-state energies (spin-state splittings) of isolated transition-metal complexes, which has shown to be a very complicated endeavour. There has been a plethora of papers describing the failure of Density Functional Theory (DFT) [7] functionals for this property [8–27], especially regarding that of B3LYP. For example, Trautwein and co-workers showed in 2001 that B3LYP is unable to correctly predict the low-spin ground-state (at 0 K) for a number of SCO complexes [11]. Reiher and co-workers subsequently proposed to lower the amount of Hartree–Fock exchange (to 15% to give the B3LYP* functional) [13,14], which seemed to perform better in many instances, but still failed dramatically for many other complexes. Other functionals had been proposed such as XLYP/X3LYP, [28] or more recently the M06 suite [29], but these were also inaccurate for the spin-state splittings [9].

An important breakthrough was made in 2004, when one of us reported for the first time the application of a new GGA functional (OPBE) to spin-state splittings [8]. This new functional combines the non-empirical PBEc correlation functional by Perdew and co-workers with Handy and Cohen's empirical OPTX exchange functional [30–32]. The spin-state splittings as predicted by OPBE give in almost all cases the correct spin ground-state [19,22,24,33–43], with as only exception the iron–porphyrin with an axial histidine ligand [44]. For this latter system OPBE predicts, like all DFT functionals, a triplet ground-state while CCSD(T) predicts a quintet ground-state, which would be more inline with experimental data. For all other systems studied so far, OPBE correctly predicts the spin ground-state, including for difficult systems like the $Fe(phen)_2(NCS)_2$ spin-crossover complex, and iron with (amp, dpa) pyridylmethylamine ligands. For these complexes, it was shown very recently that OPBE is the only DFT functional able to correctly predict a high-spin ground-state for $Fe(amp)_2Cl_2$ and a low-spin for the related $Fe(dpa)_2^{2+}$ complex [9]. Moreover, also for NMR chemical shifts and reaction barriers does OPBE seem to perform significantly better than other DFT functionals [35,36,45,46].

It should be noted also that not only the DFT functional is important, but also the basis set that is being used [47]. We recently reported a systematic study into the effect of the basis set, and found that Slater-type orbital (STO) basis sets performed well, and also very large Gaussian-type orbital (GTO) basis sets [47]. However, neither small/medium GTOs nor basis sets containing effective core potentials (ECPs) were reliable. Moreover, for a series of Pople basis sets, it was observed that the largest basis set (6-311 + G**) actually gave the largest deviation from the reference STO/very-large-GTO data. Here, we use both a reliable functional (OPBE) and reliable (STO) basis sets so that we can confide in the results obtained. In particular, we have studied the spin-state splittings for isolated $Fe(Tp^x)_2$ complexes to see how these are influenced by substituent effects on the pyrazolyl-ring.

We have studied also the neutral analogues of the anionic Tp^x ligands, i.e. the trispyrazolylmethane ligands [48]. Note that in order to distinguish the methane ligand from the borate ligand, from here on we will refer to these as T_c and T_b respectively. Despite the fact that trispyrazolylmethane was first reported in 1937 [49], its chemistry is underdeveloped in comparison with the boron counterpart. However, recent breakthroughs in the synthesis of ring-substituted trispyrazolylmethanes [50] offer the opportunity for the development of this promising class of ligand. They are formally derived by replacing the apical $(BH)^-$ anionic moiety with the isoelectronic CH group [48]. Because the T_c^x ligand is neutral, the iron(II) di-scorpionate with two T_c^x ligands has a total charge of +2, and hence in experimental studies is accompanied by one or more counter-ions. The presence of the counter-ion(s), and even which one is present, was shown to have a large influence on the stability and properties of the complex [51,52]. Nowadays, complexes with a wide range of metals supported by T_c^x ligands have been synthesized [52,53], and many studies about spin-transitions in the Fe(II) complexes have been reported [54–61]. Consequently, we decided to carry out a study on a wide range of iron(II) complexes with T_b^x and T_c^x ligands, with particular emphasis on how these are influenced by substitution patterns [51].

2. Computational

The calculations using the unrestricted formalism have been performed with the Amsterdam Density Functional (ADF) suite of program [62]. MOs were expanded in an uncontracted set of Slater type orbitals (STOs) of triple-ζ quality containing diffuse functions and one (TZP) sets of polarization functions. Energies and gradients were calculated using the local density approximation (LDA; Slater exchange and VWN correlation) with gradient-corrections (GGA) for

Table 1
Experimental data available for some of the Fe(II) complexes of trispyrazolylborate and trispyrazolylmethane studied in this article (see Scheme 3).

Complex	Spin-state or $T_{1/2}$ (K)	Form of spin-state transition	Spin states of crystal structure (*s*)	Other measurements[a]	References
$[Fe(T_b)_2]$	393 on first scan, 360 on subsequent scans	gradual	LS	Cal, IR, Mag, Möss, PES,Press, Sol, Stress, XAS	[75–77,79,85–93]
$[Fe(T_c)_2]Br_2$			LS	Mag	[94]
$[Fe(T_c)_2]X_2$ ($X^- = NO_3^-$, ClO_4^-, PF_6^-)	all > RT	all gradual	LS (NO_3^-)	ISC, Mag (NO_3^-, ClO_4^-), Möss	[60,95]
$[Fe(T_c)_2][BF_4]_2$	420	gradual	LS	Mag, Möss, XAS	[54,79]
$[Fe(T_b^{3Me})_2]$	HS at 4 K	n/a	HS	Möss, XAS	[75–77]
$[Fe(T_c^{3Me})_2]X_2$ ($X^- = NO_3^-$, BF_4^-)	175–220	both gradual		Mag, Möss	[78]
$[Fe(T_c^{3Me})_2][PF_6]_2$			HS	Mag, Möss	[78]
$[Fe(T_b^{3FMe})_2]$	HS		HS	Möss, XAS	[77,96,97]
$[Fe(T_b^{4Me})_2]$	LS			Möss	[77,92,98]
$[Fe(T_c^{4Me})_2]_2][PF_6]_2$	280	gradual		Mag, Möss	[78]
$[Fe(T_b^{4Br})_2]$	LS			Möss	[77]
$[Fe(T_c^{4Br})_2][ClO_4]_2$	355	gradual		Mag, Möss	[78]
$[Fe(T_b^{3,5\text{-}Me2})_2]$	195	gradual	HS:LS	Mag, Möss, MM, Press, Sol, XAS	[75–77,79,87,90,91,93,99,100]
$[Fe(T_c^{3,5\text{-}Me2})_2][BF_4]_2$	206	abrupt, 50% complete	2·HS, 1:1 HS:LS	Mag, Möss, Press, XAS	[54,55,57,79]
$[Fe(T_c^{3,5\text{-}Me2})_2]I_2$	203	abrupt, 15 K hysteresis, ca. 80% complete	HS	Mag, Möss, Press, XAS	[56,57]
$[Fe(T_c^{3,5\text{-}Me2})_2]I_2{\cdot}4CH_2Cl_2$	HS above 110 K		HS		[56]
$[Fe(T_c^{3,5\text{-}Me2})_2][ClO_4]_2$	HS			Mag, Möss	[78]
$[Fe(T_b^{3,4,5\text{-}Me3})_2]$	HS		HS	Mag, Möss, Press, Sol, XAS	[59,90,91,93,99,101,102]
$[Fe(T_c^{3,4,5\text{-}Me3})_2][BF_4]_2$	129	abrupt, 38 K hysteresis	HS	Mag, Möss	[58]
$[Fe(T_b^{N4})_2]$	310	gradual	LS	Mag, Möss, PES, Sol	[75,89,103]
$[Fe(T_b^{4,5\text{-}Ph})_2]$	LS		LS	Möss	[80]
$[Fe(T_b^{4,5\text{-}Ph\text{-}N3})_2]$	HS			Möss	[75]

[a] Cal = calorimetry; IR = variable temperature infrared spectroscopy; Mag = variable temperature magnetic susceptibility; MM = molecular mechanics calculations; Möss = Mössbauer spectroscopy; Press = magnetic susceptibility or Mössbauer spectroscopy measurements under high pressure; Sol = spin-crossover temperature determination in solution by variable temperature UV/Vis or Evans method measurements; stress = magnetic susceptibility measurements under mechanical stress; XAS = X-ray absorption spectroscopy (EXAFS or XANES).

exchange (OPTX) [31] and correlation (PBE) [32] included self-consistently, i.e. the OPBE functional [30]. Geometries were optimized with the QUILD program [63] using adapted delocalized coordinates [64] until the maximum gradient component was less than 1.0e-4 atomic units.

There is a fundamental difference between basis sets and effective core potentials (ECPs), which are in fact model Hamiltonians that replace the effect of the core-electrons. Here, we refer to the combination of the ECPs with their corresponding valence basis sets together as ECP Basis-sets (ECPBs). Note also that the ECP approach differs fundamentally from the frozen-core approach [65] used in ADF. Although core-electrons are not included in the SCF procedure within the frozen-core approach in ADF, it *does* include the core-orbitals and explicitly orthogonalizes the valence orbitals to them. Moreover, the core density is obtained and included explicitly, albeit with core-orbitals that are kept frozen during the SCF procedure. The influence of keeping the core-orbitals frozen within ADF is usually small (see below). Here we have frozen-core basis sets for the geometry optimizations and OPBE SCF energies, and the corresponding all-electron basis sets for post-SCF energies of other functionals.

For some complexes, an energy decomposition analysis (EDA) [66] has been performed to study the chemical bonding in these complexes. In this EDA analysis, the total energy ΔE_{total} for the heterolytic association [37] reaction between the iron(II) cation and n ligands L with charge q ($^5Fe^{2+} + n{\cdot}L^q \rightarrow FeL_n^{nq+2}$) results directly from the Kohn–Sham molecular orbital (KS–MO) model [66] and is made up of two major components: preparation and interaction. The preparation energy contains the energy needed to bring the cation and ligands together from their isolated equilibrium geometry to their positions they attain in the complex, and consists of the deformation energy ΔE_{deform}, the interaction energy between the two ligands ($\Delta E_{lig-lig}$), and the energy needed to excite the iron(II) cation from its quintuplet ground-state to the singlet/quintuplet state (with corresponding orbital occupations) it attains in the complex (ΔE_{valexc}). Note that these latter do not concur to the ones of the isolated cation, and can thus not be compared to experimental ionization energies for the iron(II) cation. Moreover, for the ground-state of the isolated iron(II) cation, we use the "average of configuration" (AOC) approach [67], which is an one-determinant approximation to the true atomic state, and serves here mainly as reference energy. The interaction energy gives the subsequent interaction between the cation on one side, and the ligands on the other, and consists of Pauli repulsion ΔE_{Pauli}, electrostatic interactions ΔE_{elstat}, and the (covalent) orbital interactions ΔE_{orbint} (see Supplementary data for full details).

The Mössbauer parameters have been calculated according to the procedure described in Refs. [68–70] with utility programs kindly provided by Han and Noodleman. The measured parameters from Mössbauer spectroscopy are isomer shift (δ), quadrupole splitting (ΔE_Q) and the metal hyperfine of ^{57}Fe sites [68–70]. The quadrupole splitting of an Fe atom arises from the non-spherical nuclear charge distribution in the $I = 3/2$ excited state, and is proportional to the electric field gradient (EFG) at the Fe nucleus, which can be calculated directly from *ab initio* molecular orbital theory and associated programs. The isomer shift is proportional to the electron density [$\rho(0)$] difference at the Fe nuclei between the studied system and a reference system (normally α-Fe at 300 K), and can then be described as [68–70]:

$$\delta = \alpha(\rho(0) - b) \Longleftrightarrow \delta = \alpha(\rho(0) - A) + C \quad (1)$$

Here, A is a constant chosen close to the electron density at the Fe nucleus in the reference state. Han and Noodleman calculated $\rho(0)$ from MO theory for a set of Fe complexes whose isomer shifts (δ_{exp}) are known experimentally, and used linear regression between the calculated $\rho(0)$ and experimental δ_{exp} values to obtain values for α and C [68–70]. With these values, the isomer shifts of other Fe compounds can be calculated directly if the same functional and basis set is used. Han and Noodleman obtained [70] the following values for OPBE/TZP for Fe(II) complexes: $\alpha = -0.318 \pm 0.049$, $C = 0.633 \pm 0.084$ mm s^{-1}, $A = 11877.0$.

The quadrupole splitting (ΔE_Q) is proportional to the electric field gradient (EFG) at the Fe nucleus. The EFG tensors (V) were obtained in single-point energy calculations with the all-electron TZP basis set. V is diagonalized and its eigenvalues reordered so that $|V_{zz}| \geq |V_{xx}| \geq |V_{yy}|$. The asymmetry parameter η is then defined as $\eta = |(V_{xx} - V_{yy})/V_{zz}|$, and finally the quadrupole splitting for ^{57}Fe can be calculated as:

$$\Delta E_Q = \frac{1}{2} eQV_{zz}(1 + \eta^2/3)^{1/2} \quad (2)$$

Here, e is the electrical charge of a positive electron, Q is the nuclear quadrupole moment (0.15 barns) of Fe. Han and Noodleman [70] did not focus on the signs of the quadrupole splittings because for many of their reference complexes, the experimental data did not report the sign, only the absolute value. Moreover, they observed that in theoretical models the sign of ΔE_Q may vary with methods of calculation and basis sets used. The main focus is therefore on the absolute values of the quadrupole splittings.

3. Results and discussion

We have studied several iron(II) complexes with the trispyrazolylborate T_b^x and trispyrazolylmethane T_c^x ligands, where substitutions have been made on the 3-, 4- and 5-position of the pyrazolyl groups (see Scheme 3 and Fig. 1). The total charge on the ligands (−1 for borate ligands, zero for methane ligands) has a substantial effect on the molecular orbitals. The highest occupied molecular orbitals of the borate ligand are found at elevated energies compared to those of the methane ligand (see Fig. S1 in the Supplementary data). As a result, the borate ligand is both more reactive and has stronger metal–ligand bonding interactions with the iron(II) ion. This leads to a larger stability of the borate complexes as compared to the methane complexes.

Table 2
Energy decomposition analysis[a,b] (kcal mol^{-1}) for singlet and quintet states of some iron complexes.

	$[Fe(T_b)_2]$		$[Fe(T_b^{3Me})_2]$		$[Fe(T_b^{3,4,5\text{-}Me3})_2]$	
	Singlet	Quintet	Singlet	Quintet	Singlet	Quintet
Preparation	259.8	97.7	271.4	103.4	267.5	104.6
ΔE_{deform}	33.8	13.1	27.7	9.5	20.4	6.1
$\Delta E_{lig-lig}$	107.8	82.7	125.5	92.0	128.9	96.6
ΔE_{valexc}	118.2	1.9	118.2	1.9	118.2	1.9
Interaction	−870.1	−701.1	−851.3	−693.5	−859.4	−705.7
ΔE_{Pauli}	441.1	136.9	366.1	114.6	362.7	122.1
ΔE_{elstat}	−647.0	−548.6	−598.5	−515.6	−596.9	−521.7
ΔE_{orbint}	−664.2	−289.4	−618.9	−292.5	−625.2	−306.1
Total	−610.3	−603.4	−579.9	−590.1	−591.9	−601.1
	$[Fe(T_c)_2]^{2+}$		$[Fe(T_c^{3Me})_2]^{2+}$		$[Fe(T_c^{3,4,5\text{-}Me3})_2]^{2+}$	
Preparation	178.9	25.9	191.7	32.5	196.0	41.4
ΔE_{deform}	24.0	7.8	20.4	6.8	15.1	5.1
$\Delta E_{lig-lig}$	36.8	16.2	53.1	23.8	62.7	34.4
ΔE_{valexc}	118.2	1.9	118.2	1.9	118.2	1.9
Interaction	−555.1	−397.4	−549.6	−401.3	−580.9	−434.5
ΔE_{Pauli}	445.4	137.6	366.7	116.3	376.2	124.0
ΔE_{elstat}	−331.3	−242.9	−298.2	−222.7	−321.9	−249.7
ΔE_{orbint}	−669.2	−292.1	−618.1	−294.9	−635.3	−308.8
Total	−376.2	−371.5	−357.9	−368.8	−384.9	−393.1

[a] Obtained at OPBE/TZ2P.
[b] See Supplementary data for a detailed discussion of these energy terms.

In order to get an estimate of the differences in metal–ligand bonding interactions in the borate and methane complexes, we have performed an energy decomposition analysis on the singlet ground-state of the parent complexes $[Fe(T_b)_2]$ and $[Fe(T_c)_2]^{2+}$ (see first column of Table 2) for the heterolytic association reaction between the iron(II) cation and n ligands L with charge q ($^5Fe^{2+} + n{\cdot}L^q \rightarrow FeL_n^{nq+2}$); see Computational details and Supplementary data for more information.

The main difference between these two complexes is observed for the electrostatic interactions between the iron(II) cation and the ligands, as was to be expected. These interactions are some 320 kcal mol^{-1} larger for the negatively charged borate ligands than for the neutral methane ligands. However, the increase in

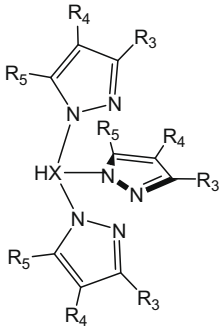

	X	R_3	R_4	R_5
T_b	B	H	H	H
T_c	C	H	H	H
T_c^{3Me}	B	CH_3	H	H
T_b^{3Me}	C	CH_3	H	H
T_c^{3FMe}	B	CF_3	H	H
T_b^{3FMe}	C	CF_3	H	H
T_c^{4Me}	B	H	CH_3	H
T_b^{4Me}	C	H	CH_3	H
T_c^{4Br}	B	H	Br	H
T_b^{4Br}	C	H	Br	H
T_c^{5Me}	B	H	H	CH_3
T_b^{5Me}	C	H	H	CH_3
T_c^{5FMe}	B	H	H	CF_3
T_b^{5FMe}	C	H	H	CF_3
$T_c^{3,5\text{-}Me2}$	B	CH_3	H	CH_3
$T_b^{3,5\text{-}Me2}$	C	CH_3	H	CH_3
$T_c^{3,4,5\text{-}Me3}$	B	CH_3	CH_3	CH_3
$T_b^{3,4,5\text{-}Me3}$	C	CH_3	CH_3	CH_3
$T_c^{3,5\text{-}Me2\text{-}4Cl}$	B	CH_3	Cl	CH_3
$T_b^{3,5\text{-}Me2\text{-}4Cl}$	C	CH_3	Cl	CH_3

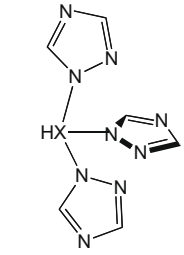

T_b^{N4}	B
T_c^{N4}	C

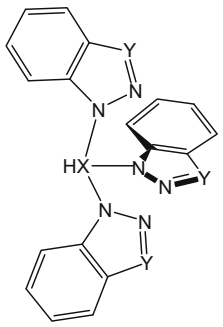

	X	Y
$T_b^{4,5\text{-}Ph}$	B	C
$T_c^{4,5\text{-}Ph}$	C	C
$T_c^{4,5\text{-}Ph\text{-}N3}$	B	N
$T_b^{4,5\text{-}Ph\text{-}N3}$	C	N

Scheme 3. Trispyrazolylborate and trispyrazolylmethane ligands studied in this work.

electrostatic interactions is compensated partly by the repulsive interactions between the two ligands (i.e. without the metal present yet), as they are brought into the position they have in the iron complex. These ligand–ligand interactions are ca. 70 kcal mol^{-1} more repulsive for the charged borate ligands than for the methane ligands (see $\Delta E_{lig-lig}$ in Table 2).

The covalent interactions between the iron and its ligating nitrogen atoms are hardly affected, as is shown by the orbital interactions term (ΔE_{orbint} in Table 2) that is found at −664 and −669 kcal mol^{-1}, respectively for the borate and methane complex. Therefore, the direct (covalent) bonding to iron is similar for both ligands, but the stability of the complex (indicated by the total energy in the table) is largely affected by the total charge of the ligands. This stability is completely governed by the electrostatic interactions, and leads to a difference of some 230 kcal mol^{-1} in favor of the borate complex. The interaction with counter-ions in case of the methane ligands will somewhat reduce this difference, but much will depend on where the counter-ions are located and which counter-ions are present. Experimental data confirm this explicit dependence of the stability on the type of counter-ion (*vide supra*).

3.1. Comparison with previous results

For a number of complexes, there are studies present in the literature that were obtained with other DFT functionals. For instance, the iron(II) complexes with the T_c, T_c^{3Me}, T_c^{4Me} and T_c^{4Br} ligands had been studied [71] with a number of DFT functionals (B3LYP, B3LYP*, BLYP, PW91) and Hartree–Fock, and a small-GTO (6-311G) basis set. As shown previously [47], such a basis set gives unreliable results for spin-state splittings. We have therefore recalculated the singlet–quintet splittings (see Table 3) for a number of DFT functionals with a reliable STO basis set (TZP).

As anticipated and consistently with previous studies, the OPBE functional predicts the correct spin ground-state for all four complexes. Moreover, the deviations from the "experimental" values (as reported in Ref. [71]) are very small (0.5–1.7 kcal mol^{-1}). The other DFT functionals have much larger deviations, but the significance of the "experimental" values for the isolated complexes in the gas-phase is uncertain. Our data show the typical behavior for spin-state splittings. Early GGAs like BLYP or PBE, and including the more recent XLYP and TPSS functionals, overestimate the stability of the low-spin state, while the hybrid functionals overestimate high-spin state stabilities. Apart from OPBE, there are two other functionals (TPSSh and M06-L) that give reasonable values, with the rest clearly giving less accurate results. This concurs with a recent benchmark study by one of us [9], where the superior performance of OPBE was already shown. One of the referees correctly pointed out that if one adds the BLYP and B3LYP data, one more or less obtains the OPBE data (see Table 3). Thus, at least for the spin-state splittings reported here, it seems that such a 1:1 combination of BLYP and B3LYP should give good results, similar to OPBE, only much slower.

The influence of the basis set is once again shown to be as significant as the choice of the DFT functional itself. For instance, there is a difference of between 4 and 13 kcal mol^{-1} between our data with the STO basis, and the data from Ref. [71] that were obtained with the inadequate 6-311G basis (see Table 3). Note that the basis set not only affects the energy, but also the geometry with lower accuracy obtained for small-GTOs than for STOs [47]. Curiously, the B3LYP splitting for $Fe(T_c)_2^{2+}$ as obtained with the 3-21G basis [11] (−7.4 kcal mol^{-1}) is closer to the STO result (−12.4 kcal mol^{-1}) than the one obtained with the 6-311G basis (−1.7 kcal mol^{-1}). However, our previous study [47] already showed that increasing the basis set size of Pople-type GTOs is not always favorable, and often actually deteriorates the result.

Long and co-workers [72] studied the parent $Fe(T_b)_2$ compound and some ring-substituted ones with the B3LYP functional and a number of GTO and/or ECPB basis sets. With an ECPB basis for iron they obtained an almost zero singlet–quintet splitting, which seems odd given that the complex stays low-spin up until 420 K. Therefore, it would be anticipated that there is a substantial singlet–quintet splitting. Indeed, this spin-state preference is correctly reflected in our OPBE data that places the quintet state higher in energy by 6 kcal mol^{-1}. Therefore, the failure of B3LYP as well as the success of OPBE for these spin-state splittings is once again shown.

3.2. Spin-state splittings with parent ligands T_b and T_c

The energy decomposition analysis described above has been performed for the singlet spin-state, which is the ground-state for the parent $[Fe(T_b)_2]$ and $[Fe(T_c)_2]^{2+}$ complexes. The triplet and quintet states are higher in energy for both these complexes by 4–30 kcal mol^{-1} (see Table 4). These energies have been obtained with the appropriate (relaxed) geometries for each of the spin-states, i.e. the geometry of each spin-state was allowed to relax fully. This leads to significant differences in metal–ligand distances, which e.g. for complex $[Fe(T_b)_2]$ are on average 1.96 Å (singlet), 2.08 Å (triplet) and 2.21 Å (quintet) (see Table S1).

Table 3
Spin-state splittings (kcal mol^{-1})[a] for a number of complexes and DFT functionals using TZP(ae) basis set.

	Type	$Fe(T_c)_2^{2+}$	$Fe(T_c^{3Me})_2^{2+}$	$Fe(T_c^{4Me})_2^{2+}$	$Fe(T_c^{4Br})_2^{2+}$
OPBE	*gga*	+3.8	−13.4	+3.8	+2.7
LDA	*lda*	+55.7	+47.4	+55.6	+54.1
PBE	*gga*	+21.9	+12.1	+21.8	+20.8
TPSS	*mgga*	+22.9	+13.1	+22.9	+21.9
TPSSh	*mgga-hybr*	+7.7	−1.1	+7.9	+7.2
PBE0	*hybr*	−15.5	−22.8	−15.1	−15.1
BLYP	*gga*	+15.3 (19.6[b])	+6.2 (9.3[b])	+15.2 (19.8[b])	+14.4 (18.9[b])
B3LYP	*hybr*	−12.4 (−1.7[b])	−19.3 (−9.6[b])	−12.1 (−1.4[b])	−12.1 (−1.9[b])
B3LYP*	*hybr*	−2.4 (5.0[b])	−9.8 (3.1[b])	−2.2 (5.3[b])	−2.5 (4.8[b])
XLYP	*gga*	+13.1	+4.4	+13.1	+12.3
X3LYP	*hybr*	−14.0	−20.4	−13.6	−13.6
M06−L	*mgga*	+6.6	−2.6	+7.1	+6.8
M06	*mgga−hybr*	−8.4	−14.4	−7.9	−7.6
"exp."[c]		+4.3	n/a[d]	+5.5	+4.3

[a] Given here is *E*(quintet)−*E*(singlet), as calculated post-SCF on OPBE/TZP(ae) orbitals and densities.
[b] Values from Ref. [71], obtained with inaccurate 6-311G GTO-basis.
[c] "Experimental" value is inaccessible for isolated complex in gas-phase (see text), value given is rough estimate as presented in Ref. [71].
[d] Not available in Ref. [71], no spin-transition observed, high-spin expected at 0 K.

Table 4
Spin-state splittings (kcal mol^{-1}) for the studied complexes.

Compound	Energy (kcal mol^{-1})			
	Singlet	Triplet	Quintet	Exp.
$[Fe(T_b)_2]$	0.0	29.7 (19.3)[a]	6.0	LS
$[Fe(T_c)_2]^{2+}$	0.0	28.4 (18.5)[a]	3.8	LS
$[Fe(T_b^{3Me})_2]$	10.5	30.9	0.0	HS
$[Fe(T_c^{3Me})_2]^{2+}$	11.2	31.1	0.0	LS/HS[b]
$[Fe(T_b^{3FMe})_2]$	21.7	35.4	0.0	HS
$[Fe(T_c^{3FMe})_2]^{2+}$	13.7	31.2	0.0	-
$[Fe(T_b^{4Me})_2]$	0.0	29.5	5.7	LS
$[Fe(T_c^{4Me})_2]^{2+}$	0.0	28.4	4.1	LS
$[Fe(T_b^{4Br})_2]$	0.0	28.7	5.1	LS
$[Fe(T_c^{4Br})_2]^{2+}$	0.0	27.5	3.0	LS
$[Fe(T_b^{5Me})_2]$	0.0	30.5	8.2	
$[Fe(T_c^{5Me})_2]^{2+}$	0.0	29.3	6.5	
$[Fe(T_b5FMe)_2]$	0.0	33.3	14.1	
$[Fe(T_c^{5FMe})_2]^{2+}$	0.0	32.3	12.7	
$[Fe(T_b^{3,5\text{-}Me2})_2]$	7.9	29.4	0.0	LS/HS
$[Fe(T_c^{3,5\text{-}Me2})_2]^{2+}$	8.2	29.4	0.0	LS/HS
$[Fe(T_b^{3,4,5\text{-}Me3})_2]$	9.7	30.0	0.0	HS
$[Fe(T_c^{3,4,5\text{-}Me3})_2]^{2+}$	8.7	29.2	0.0	LS
$[Fe(T_b^{3,5\text{-}Me2\text{-}4Cl})_2]$	9.5	29.9	0.0	
$[Fe(T_c^{3,5\text{-}Me2\text{-}4Cl})_2]^{2+}$	8.9	29.2	0.0	
$[Fe(T_b^{N4})_2]$	0.0	29.9	5.6	LS
$[Fe(T_c^{N4})_2]^{2+}$	0.0	27.7	2.4	
$[Fe(T_b^{4,5\text{-}Ph})_2]$	0.0	33.1	12.8	LS
$[Fe(T_c^{4,5\text{-}Ph})_2]^{2+}$	0.0	30.3	8.0	
$[Fe(T_b^{4,5\text{-}Ph\text{-}N3})_2]$	0.0	36.9	18.5	HS
$[Fe(T_c^{4,5\text{-}Ph\text{-}N3})_2]^{2+}$	0.0	35.2	16.3	

[a] Value in parentheses obtained with lower symmetry (Jahn–Teller distorted).
[b] Dependent on counter-ion.

These calculations have been performed with D_{3d} symmetry imposed on the geometry, which concurs with the symmetry observed for the experimental structure (in the singlet ground-state). However, in the triplet state, the occupations of the molecular orbitals are not optimal within this symmetry restriction, i.e. two degenerate orbitals within the e_g irrep are each occupied by half an electron.

This leads to Jahn–Teller distortions, in which through symmetry lowering the iron–ligand distances are no longer equivalent. Usually for a pseudo-octahedral coordination around the metal, after Jahn–Teller distortion the distances to the four equatorial ligands remain similar, while the two axial ligands show significant changes, either to longer or shorter distances. Although the issue of Jahn–Teller distortion is only relevant for the high-lying triplet state, and the relaxation in lower symmetry usually contributes only a few kcal mol^{-1} of stabilization, we also performed calculations for the triplet states within C_{2h} symmetry. This symmetry allows the axial ligands to have different distances to the metal than the equatorial ligands. Indeed, the axial metal-distances change significantly to 2.41 Å ($[Fe(T_b)_2]$) and 2.39 Å ($[Fe(T_c)_2]^{2+}$), while the equatorial ligands are found at 1.98 Å (for both complexes). Nevertheless, the additional stabilization of 10.4 ($[Fe(T_b)_2]$) and 9.9 ($[Fe(T_c)_2]^{2+}$) kcal mol^{-1} is only minor compared to the initial destabilization with respect to the ground-state, i.e. after Jahn–Teller distortions these triplet states remain ca. 19 kcal mol^{-1} higher in energy than the singlet ground-state. Therefore, hereafter we focus only on the low-spin singlet and high-spin quintet states that are much closer in energy.

3.3. Influence of substituents on spin ground-state

If we replace the H atoms in the 3-pyrazolyl-rings' position with the bulkier methyl groups (T_x^{3Me}), the intraligand and interligand repulsions are significantly enhanced. In fact, the interligand repulsions act effectively in a way as to lengthen the Fe–N bond distances in order to be relieved. This is clearly the case in our calculations where the iron–nitrogen distances increase by ca. 0.05 Å for all three spin states (compare $Fe(T_b)_2$ and $Fe(T_b^{3Me})_2$ in Table S1). It should also be mentioned that inversions of pyrazole rings are a well documented phenomenon when an isopropyl group is positioned at position 3 of the pyrazolyl group in the ligand [73,74]. This may lead to the rotation of one of the pyrazolyl groups, thereby putting the isopropyl at the 5-position in order to reduce steric interactions, and one thus obtains a mixed 3-Me, 3-Me, 5-Me ligand. Moreover, our EDA analysis for these two complexes clearly shows a larger repulsive interaction between the ligands in case of the T_b^{3Me} ligand (see $\Delta E_{lig-lig}$ in Table 2). The increase of this repulsion is clearly larger for the singlet (from 107.8 to 125.5 kcal mol^{-1}) than for the quintet (from 82.7 to 92.0 kcal mol^{-1}). Although this undoubtedly favors the HS state, it may or may not be sufficient for leading to an inversion of the spin-state stabilities.

The increase of ligand–ligand repulsion is counteracted by the deformation energy that shows a larger decrease for the singlet (33.8 to 27.7 kcal mol^{-1}) than for the quintet (13.1 to 9.5 kcal mol^{-1}). Taken these two counteracting effects into account leads to an overall effect of 5.9 kcal mol^{-1} in favor of the quintet state (see preparation energy). However, an even larger effect comes from the interaction energy that decreases by 18.8 kcal mol^{-1} for the singlet state and only 7.6 kcal mol^{-1} for the quintet state, i.e. 11.2 kcal mol^{-1} in favor of the quintet. All three components of the interaction energy are important for this decrease, i.e. for the singlet state the Pauli repulsion (ΔE_{Pauli}) decreases by 75.0 kcal mol^{-1}, the electrostatic interactions (ΔE_{elstat}) decrease by 48.5 kcal mol^{-1}, and the orbital interactions (ΔE_{orbint}) by 45.3 kcal mol^{-1}. On the other hand for the quintet, ΔE_{Pauli} repulsion decreases by 22.3 kcal mol^{-1}, ΔE_{elstat} by 33 kcal mol^{-1}, while the orbital interactions actually increase by 3.1 kcal mol^{-1}.

The introduction of the methyl groups therefore has a number of effects that are interrelated: (i) larger ligand–ligand repulsion; (ii) larger iron–ligand distances; (iii) smaller metal–ligand bonding interactions. Of these effects, the third has the largest effect on the spin-state splitting and not, as anticipated from experimental studies, the first, although the ligand–ligand repulsion is the driving force that leads to the larger iron–ligand distances and hence the smaller metal–ligand bonding.

The same pattern is observed for the corresponding pyrazolylmethane ligands (T_c and T_c^{3Me}), where the introduction of the methyl groups at the 3-position leads to an increase of the iron–ligand distances. At the same time an increase of ligand–ligand repulsion is observed, which is again larger for the singlet (from 36.8 to 53.1 kcal mol^{-1}, see Table 2) than for the quintet (16.2 to 23.8 kcal mol^{-1}). However, the metal–ligand interactions are even more affected, which *decrease* for the singlet state (from −555.1 to −549.6 kcal mol^{-1}) and *increase* for the quintet state (from −397.4 to −401.3 kcal mol^{-1}). These patterns are very similar to those of the corresponding borate complexes (see above), which reiterates our finding that covalent (direct) metal–ligand interactions are very similar between a borate (T_b^x) complex and its corresponding methyl (T_c^x) complex.

Placing the methyl groups at other positions of the pyrazolyl-ring has no effect on the spin ground-state, which remains the singlet. The spin-state splitting is hardly affected when placing a methyl group at the 4-position (difference with parent compound ca. 0.3 kcal mol^{-1}, see Table 4), and is only slightly increased by 2–3 kcal mol^{-1} when placing it at the 5-position (see $Fe(T_b^{5Me})_2$ and $Fe(T_c^{5Me})_2^{2+}$ in Table 4). Moreover, even when the 4-position of the pyrazolyl-rings of the trispyrazolylborate ligands is occupied by an isopropyl (i-Pr) substituent, the complex shows the same spin behavior as $[Fe(T_b)_2]$, indicating that the steric hindrance is not important [75].

Replacing the C4–H group by a nitrogen (in the T_b^{N4} and T_c^{N4} ligands) also does not have a significant effect on the spin-state splittings. On the other hand, replacing the hydrogens on the methyl group by fluorines has a stabilizing effect on the ground-state. For instance, the spin-state splitting of 10.5 kcal mol^{-1} in favor of the quintet for the T_b^{3Me} ligand increases to 21.7 kcal mol^{-1} for the T_b^{3FMe} ligand. Likewise, the splitting of 8.2 kcal mol^{-1} in favor of the singlet state for the T_b^{5Me} ligand increases to 14.1 kcal mol^{-1} for the T_b^{5FMe} ligand. Therefore, the introduction of fluorines by itself does not lead to a preference for either low- or high-spin, but merely enhances the ground-state.

The simultaneous introduction of two or three methyl groups at the pyrazolyl-ring leads to only small changes compared to the T_x^{3Me} ligand. In all cases is a high-spin ground-state observed, but the spin-state splitting varies somewhat. For T_b^{3Me} it was 10.5 kcal mol^{-1} in favor of the quintet, which reduces to 7.9 kcal mol^{-1} for $T_b^{3,5\text{-}Me2}$, and then increases back to 9.7 kcal mol^{-1} for $T_b^{3,4,5\text{-}Me3}$ (see Table 4). Interestingly enough, this change in spin-state splitting is now almost entirely resulting (compare $Fe(T_b^{3,4,5\text{-}Me3})_2$ and $Fe(T_b)_2$ in Table 2) from metal–ligand interactions, and hardly any effect is coming from the preparation energy (i.e. direct ligand–ligand repulsion and deformation energy).

3.4. Comparison between spin-state splittings and spin-crossover behavior

Evidence for spin-crossover (SCO) behavior is often obtained by looking at magnetic susceptibility data and/or Mössbauer spectra (see below), which are then associated with the spin-state preferences for the transition-metal complexes. However, SCO behavior results from cooperative effects of a large number of TM-complexes, and hence, these collective spin-state preferences do not necessarily reflect the preference of one individual TM-complex. In order to test in how far these two are correlated, we can now compare our computed spin-state splittings with the experimentally observed ones (see Table 4).

The low-spin ground-state of the parent complexes $Fe(T_b)_2$ and $Fe(T_c)_2^{2+}$ is observed both for an individual complex (as evidenced by our calculations) and for a cluster of complexes in the solid-state phase (experiment). Likewise, the high-spin ground-state of the 3-methyl analogues is present in both the theoretical and experimental systems [75–77]. It should be noted however that for the T_c^{3Me} ligand the experimental spin-state seems to depend on the kind of counter-ion that is present [78]. With PF_6^- and BF_4^- counter-ions a low-spin is observed, while with ClO_4^- a predominantly high-spin state is observed [78].

For most other complexes, the spin ground-state of an individual TM-complex (from our OPBE data) coincides with the experimentally observed spin-state (for the solid-state) [75]. There are however two exceptions, which are observed when more than one methyl group substituent is present. For instance, for the $T_x^{3,5\text{-}Me2}$ and $T_x^{3,4,5\text{-}Me3}$ ligands our computational data clearly indicate a high-spin ground-state. This is for the $T_c^{3,5\text{-}Me2}$ methane-complex corroborated by experimental data at 4.2 K with a ClO_4^- counter-ion present. However, with the BF_4^- counter-ion a mixture of collective high-spin and low-spin states is observed [54,79]. Moreover, with the iodide counter-ion, sample dependent spin-crossover or no-crossover is observed, which seems to also depend on the presence of absence of solvent (CH_2Cl_2) molecules in the crystalline sample [56]. All this indicates clearly that the chemical environment of the $Fe(T_c^{3,5\text{-}Me2})_2^{2+}$ di-cation in the ionic lattice influences the spin-crossover severely, and any collective spin-state thus obtained does not reflect the spin ground-state of an individual di-cation. For the $T_b^{3,5\text{-}Me2}$ ligand one obtains either a collective low-spin state in the experiments, or a mixture of low- and high-spin states depending on the crystallization process [75].

For the $T_b^{3,4,5\text{-}Me3}$ ligand a collective high-spin state is observed, both by theory and experiment [75]. On the other hand, the solid-state structure and color of $[Fe(T_c^{3,4,5\text{-}Me3})_2](BF_4)_2$ clearly show that the complex contains high-spin iron(II) at ambient temperature, but both magnetic and Mössbauer studies point out that the complex rapidly and completely changes to the low-spin state below 100 K [58]. This would indicate that for the first time there is a significant difference between a methane and its corresponding borate complex, which in all other cases shows a similar spin ground-state in the experiments and in our calculations. In fact, also in this case do our calculations give a similar (HS) ground-state for $[Fe(T_b^{3,4,5\text{-}Me3})_2]$ and $[Fe(T_c^{3,4,5\text{-}Me3})_2]^{2+}$. Since our EDA analysis indicated for complexes $[Fe(T_b)_2]$ and $[Fe(T_c)_2]^{2+}$ that the covalent bonding was similar in these two complexes (see above), we were wondering if there was a change for the complexes $[Fe(T_b^{3,4,5\text{-}Me3})_2]$ and $[Fe(T_c^{3,4,5\text{-}Me3})_2]^{2+}$. However, similar to the situation for the T_b and T_c ligands, our results show that the metal–ligand interactions are similar (see Table 2).

3.5. Mössbauer parameters

We have calculated the Mössbauer parameters for all transition-metal complexes with the T_b^x and T_c^x ligands, and find the usual distinction between the isomer shifts and quadrupole splittings of the singlet state versus those of the quintet state (see Table 5). For instance, the isomer shifts of the singlet states are found at lower values (0.5–0.7 mm s^{-1}) than those of the quintet states (1.0–1.2 mm s^{-1}). Likewise, the quadrupole splitting is found at lower values for the singlet (between −0.4 and 0.1 mm s^{-1}) than for the quintet (between −3.4 and −3.7 mm s^{-1}). However, we did not find any clear correlation between these Mössbauer parameters and substituent patterns. It should be mentioned however that especially the isomer shift is very similar between the borate and methane ligands. For instance, that of $Fe(T_b)_2$ is found at 0.605 mm·s^{-1} and that of $Fe(T_c)_2^{2+}$ at 0.607 mm s^{-1}. Placing a methyl group at the 3-position increases these values to 0.711 and 0.707 mm s^{-1} (see Table 5), while placing a methyl group at the 4- or 5-position has only a very modest effect (as was also evident from the spin-state splittings).

3.6. Poly-indazole ligands

A drastically different substitution pattern is present in the $[Fe(T_b^{4,5\text{-}Ph})_2]$ and $[Fe(T_c^{4,5\text{-}Ph})_2]^{2+}$ complexes, where carbons 4 and 5 of the pyrazolyl-ring also form part of an attached phenyl ring (see Scheme 3) that together form an indazole group. These poly(indazole)borate systems are of interest because of the two possible regio-isomeric structures [80]. The B–N formation can occur at the nitrogen atom N1 or N2 (by indazole numbering, see Scheme 4, left and right, respectively). The latter isomer is the empirically expected form where B–N bond formation (from KBH_4 and indazole) had occurred at the least-hindered nitrogen [56]. Interestingly however, this isomer (on the right in Scheme 4) appears to be encountered only with 7-substituted indazoles [81,82]. With unsubstituted or otherwise substituted indazoles the isomer where the boron is coordinated to N1 (left in Scheme 4) is formed, probably because of electronic reasons [56]. It is most likely governed by the aromaticity of the ligands, which is larger for the left isomer than for the right isomer. This is indicated by the Harmonic Oscillator Model of Aromaticity (HOMA) [83] values that are found to be 0.826 (five-membered ring) and 0.900 (phenyl group) for the left isomer, and 0.852 (five-membered ring) and 0.804 (phenyl) for the right isomer; larger HOMA values indicate larger aromaticity and hence larger stability. These HOMA values

Table 5
Experimental and computed isomer shift (IS) and quadrupole splitting (QS) for the complexes studied (mm s^{-1}).

Complex	T (K)	$IS_{exp.}$	$QS_{exp.}$	Pct.[a]	GS[b]	References	IS_{LS}[c]	QS_{LS}[c]	IS_{HS}[d]	QS_{HS}[d]
$[Fe(T_b)_2]$	293	0.40	0.20	100	$^1A_{1g}(O_h)$	[75]	0.605	0.001	1.130	−3.565
	4.2	0.48	0.22	100	$^1A_{1g}(O_h)$					
$[Fe(T_c)_2]^{2+}$	472	0.74	2.98	100	$^5T_{2g}(O_h)$	[56]	0.607	0.073	1.136	−3.631
	4.2	0.45	0.25	100	$^1A_{1g}(O_h)$					
$[Fe(T_b^{3Me})_2]$	4.2	0.45	0.21	20	$^1A_{1g}(O_h)$	[75]	0.711	−0.167	1.171	−3.408
	4.2	1.06	3.81	58	$^5T_{2g}(O_h)$					
$[Fe(T_c^{3Me})_2]^{2+}$	4.2	0.53[e], 0.53[f]	0.43[e], 0.36[f]		$^1A_{1g}(O_h)$	[78]	0.707	−0.031	1.167	−3.545
	4.2	1.24[e], 1.13[f]	3.71[e], 3.99[f]		$^5T_{2g}(O_h)$					
$[Fe(T_b^{3FMe})_2]$	293	1.11	3.49	100	$^5T_{2g}(O_h)$	[77]	0.849	−0.358	1.190	−3.024
	4.2	1.11	3.49	100	$^5T_{2g}(O_h)$					
$[Fe(T_c^{3FMe})_2]^{2+}$							0.769	−0.248	1.179	−3.149
$[Fe(T_b^{4Me})_2]$	293	0.39	0.34	100	$^1A_{1g}(O_h)$	[77]	0.608	0.014	0.986	−3.374
$[Fe(T_c^{4Me})_2]^{2+}$	[g]	0.51	0.32		$^1A_{1g}(O_h)$	[78]	0.613	0.077	1.139	−3.611
	[g]	0.97	3.55		$^5T_{2g}(O_h)$					
$[Fe(T_b^{4Br})_2]$	293	0.37	0.56	100	$^1A_{1g}(O_h)$	[77]	0.621	0.025	1.131	−3.508
$[Fe(T_c^{4Br})_2]^{2+}$	[g]	0.48	0.35		$^1A_{1g}(O_h)$	[78]	0.630	0.108	1.144	−3.599
	[g]	1.41	3.12		$^5T_{2g}(O_h)$					
$[Fe(T_b^{5Me})_2]$							0.593	0.037	1.112	−3.571
$[Fe(T_c^{5Me})_2]^{2+}$							0.596	0.113	1.121	−3.656
$[Fe(T_b^{5FMe})_2]$							0.533	−0.040	1.063	−3.526
$[Fe(T_c^{5FMe})_2]^{2+}$							0.528	0.076	1.069	−3.690
$[Fe(T_b^{3,5\text{-}Me2})_2]$	4.2	0.56	0.11	58	$^1A_{1g}(O_h)$	[75]	0.695	−0.137	1.154	−3.411
	4.2	1.03	3.66	42	$^5T_{2g}(O_h)$					
$[Fe(T_c^{3,5\text{-}Me2})_2]^{2+}$	190	1.02	3.86	100	$^1A_{1g}(O_h)$	[56]	0.686	0.016	1.148	−3.590
	4.2	0.46	0.21	100	$^5T_{2g}(O_h)$					
$[Fe(T_b^{3,4,5\text{-}Me3})_2]$	293	1.05	3.72	100	$^5T_{2g}(O_h)$	[75]	0.718	−0.133	1.152	−3.397
	4.2	1.20	3.71	100	$^5T_{2g}(O_h)$					
$[Fe(T_c^{3,4,5\text{-}Me3})_2]^{2+}$	160	1.09	3.92	100	$^5T_{2g}(O_h)$	[58]	0.696	−0.016	1.154	−3.505
	4.2	0.52	0.20	100	$^1A_{1g}(O_h)$					
$[Fe(T_b^{3,5\text{-}Me2\text{-}4Cl})_2]$	293	0.33	0.77	15	$^1A_{1g}(O_h)$	[75]	0.617	−0.116	1.136	−3.356
	293	1.00	3.68	85	$^5T_{2g}(O_h)$					
$[Fe(T_c^{3,4,5\text{-}Me3})_2]^{2+}$							0.704	0.017	1.146	−3.499
$[Fe(T_b^{N4})_2]$	293	0.32	0.07	100	$^1A_{1g}(O_h)$	[75]	0.691	−0.048	1.152	−3.572
	4.2	0.39	0.18	100	$^1A_{1g}(O_h)$					
$[Fe(T_c^{N4})_2]^{2+}$							0.634	0.025	1.143	−3.659
$[Fe(T_b^{4,5\text{-}Ph})_2]$	287	0.34	0.16	100	$^1A_{1g}(O_h)$	[80]	0.582	−0.123	1.127	−3.601
$[Fe(T_c^{4,5\text{-}Ph})_2]^{2+}$							0.603	0.019	1.141	−3.635
$[Fe(T_b^{4,5\text{-}Ph\text{-}N3})_2]$	4.2	0.26	0.68	4	$^1A_{1g}(O_h)$	[75]	0.511	−0.248	1.119	−3.569
	4.2	1.09	2.92	96	$^5T_{2g}(O_h)$					
$[[Fe(T_c^{4,5\text{-}Ph\text{-}N3})_2]^{2+}$							0.514	−0.116	1.124	−3.626

[a] Percentage assigned to spin-states.
[b] Spin-state assignation in terms of idealized O_h symmetry.
[c] Computed at OPBE/TZP for low-spin state.
[d] Computed at OPBE/TZP for high-spin state.
[e] With counter-ion ClO_4^-.
[f] With counter-ion BF_4^-.
[g] Low temperature.

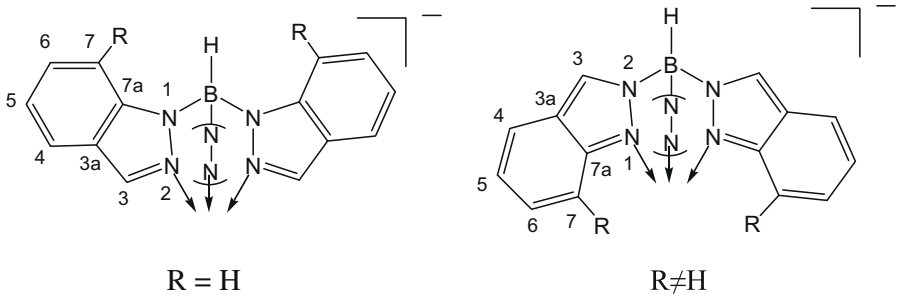

Scheme 4. Regio-isomeric structures for the hydrotris(indazol-1-yl)borato ligand ($T_b^{4,5\text{-}Ph}$). –(N–N)– denotes the indazolyl ring which is oriented to the rear.

are corroborated by the stability of the ligands at the OPBE/TZP level, which shows that the left isomer is more stable than the right one by 5.0 kcal mol^{-1}.

For this regio-isomeric structure, boron is bonded to the sterically more hindered but electronically richer nitrogen atom, which leads to the negatively charged $T_b^{4,5\text{-}Ph}$ ligand. The experimental collective spin-state of $[Fe(T_b^{4,5\text{-}Ph})_2]$ in the solid-state is low-spin, which agrees with the theoretical results for the isolated complex. The $[Fe(T_c^{4,5\text{-}Ph})_2]^{2+}$ complex has not been synthesized experimentally yet, but we predict that its ground-state would also be the singlet spin state.

In the complex $[Fe(T_b^{4,5\text{-}Ph\text{-}N3})_2]$, with benzatriazole groups in which the 3-position of the pyrazolyl-ring is also occupied by a nitrogen (see Scheme 3), the presence of the low-spin isomer in

the solid-state is not more than 4%, even at the liquid nitrogen temperature [75]. The coordination of 3-N for the $T_b^{4,5\text{-Ph}-N3}$ ligand, which is a better donor than 2-N, would allow polymeric structures to be formed. Our calculations predict clearly that the ground-state of an individual $Fe(T_b^{4,5\text{-Ph}-N3})_2$ complex should be a singlet, which differs from the spin-state of the solid-state phase of the complex that indicate a high-spin state. In fact, for this complex we observe the largest splitting between the singlet and quintet state, of 18.5 kcal mol^{-1}.

Although it was already shown above that the chemical environment plays a large part in the determination of the collective spin-state in the solid-state, we were intrigued by the apparent difference between the spin-state of one $[Fe(T_b^{4,5\text{-Ph}-N3})_2]$ complex and that of the solid-state equivalent. Since the crystallographic structure of $[Fe(T_b^{4,5\text{-Ph}-N3})_2]$ has not been obtained, it is not possible to know exactly the structure of the complex for which the experimental data had been obtained. Therefore, we have studied a number of possible alternative structures: one where iron is for instance bonded to N3 instead of N2; the other regio-isomeric structure (see Scheme 4); with a different number of ligands (four instead of six); or other exotic structures in which indazole groups of the top ligand are stacked above each other, or above indazole groups of the bottom ligand. However, neither of these trials resulted in a more stable structure than the "standard" D_{3d} oriented structure that was observed for most of the other complexes. Note also that the experimental Mössbauer quadrupole splitting of the HS state of 2.92 mm s^{-1} is significantly smaller than those observed for the other complexes, which are usually observed between 3.5 and 3.9 mm s^{-1}. Our computed quadrupole splitting for the D_{3d} structure is indeed similar to those of the other complexes, giving further credibility to the hypothesis that the experimental data do not correspond to this D_{3d} structure, nor to its crystalline solid-state equivalent.

A possible explanation for the difference between our computed values for one individual $[Fe(T_b^{4,5\text{-Ph}-N3})_2]$ complex (LS) and the experimentally observed (HS) spin-state might be given by a recent experimental study. In it, a penta-nuclear iron(III) complex with four benzotriazole and a number of other ligands has been reported, which was found with a HS ground-state [84]. Taken together with the possible formation of polymers [75] and our compelling evidence of a LS ground-state for $[Fe(T_b^{4,5\text{-Ph}-N3})_2]$, this might indicate that the Mössbauer parameters from Ref. [75] would not correspond to this mono-nuclear iron(II) complex but instead to an oligo- or poly-nuclear structure.

4. Conclusions

We have studied the spin-state preferences of iron(II) complexes with trispyrazolylborate and trispyrazolylmethane ligands, and determined at the OPBE/TZP level how these for an individual iron(II) complex in the gas-phase are influenced by substitution patterns at the pyrazolyl-ring. By using an energy decomposition analysis of the metal–ligand and ligand–ligand interactions, we have shown that there is strong resemblance between the covalent metal–ligand interactions for both ligands. However, the total stability of the complexes is greatly enhanced for the overall neutral borate complexes compared to the corresponding methane complexes, which results as anticipated mostly from differences in electrostatic interactions. This may explain why in experiments such a large dependence on the presence, location and nature of counter-ions is observed. Apart from these effects, there is generally a strong resemblance between the spin ground-state of an individual iron(II) complex in the gas-phase, and the collective spin-state of an ensemble of complexes in the solid-state.

The spin-state preferences of the individual iron(II) complexes are shown to be determined mainly by methyl groups at the 3-position of the pyrazolyl-rings. Its presence leads to intra-molecular interligand repulsion that leads to larger iron–ligand distances. This leads to a sharp reduction of favorable metal–ligand bonding interactions, whose loss is mainly responsible for the change in spin-state preferences of the complexes.

Acknowledgments

This study was financially supported by the Spanish research projects CTQ2008-03077/BQU and CTQ2008-06532/BQU and the DURSI project nr. 2005SGR-00238. MG thanks MEC for a research grant. We thank W. Han and L. Noodleman for providing the utility programs to compute the Mössbauer parameters of the iron complexes.

Appendix A. Supplementary data

Supplementary data associated with this article can be found, in the online version, at doi:10.1016/j.poly.2009.06.006.

References

[1] S. Trofimenko, J. Am. Chem. Soc. 88 (1966) 1842.
[2] S. Trofimenko, Chem. Rev. 93 (1993) 943.
[3] S. Trofimenko, Scorpionates. The Coordination Chemistry of Polypyrazolylborate Ligands, Imperial College Press, London, 1999.
[4] J.P. Jesson, S. Trofimenko, D.R. Eaton, J. Am. Chem. Soc. 89 (1967) 3158.
[5] T. Buchen, P. Gütlich, Inorg. Chim. Acta 231 (1995) 221.
[6] J.W. Turner, F.A. Schultz, J. Phys. Chem. B 106 (2002) 2009.
[7] W. Koch, M.C. Holthausen, A Chemist's Guide to Density Functional Theory, Wiley-VCH, Weinheim, 2000.
[8] M. Swart, A.R. Groenhof, A.W. Ehlers, K. Lammertsma, J. Phys. Chem. A 108 (2004) 5479.
[9] M. Swart, J. Chem. Theory Comput. 4 (2008) 2057.
[10] A.R. Groenhof, M. Swart, A.W. Ehlers, K. Lammertsma, J. Phys. Chem. A 109 (2005) 3411.
[11] H. Paulsen, L. Duelund, H. Winkler, H. Toftlund, A.X. Trautwein, Inorg. Chem. 40 (2001) 2201.
[12] K.P. Jensen, Inorg. Chem. 47 (2008) 10357.
[13] M. Reiher, O. Salomon, B.A. Hess, Theor. Chem. Acc. 107 (2001) 48.
[14] M. Reiher, Inorg. Chem. 41 (2002) 6928.
[15] A. Ghosh, J. Biol. Inorg. Chem. 11 (2006) 712.
[16] A. Ghosh, P.R. Taylor, Curr. Opin. Chem. Biol. 7 (2003) 113.
[17] I.H. Wasbotten, A. Ghosh, Inorg. Chem. 46 (2007) 7890.
[18] J. Conradie, D.A. Quarless, H.F. Hsu, T.C. Harrop, S.J. Lippard, S.A. Koch, A. Ghosh, J. Am. Chem. Soc. 129 (2007) 10446.
[19] I. Wasbotten, A. Ghosh, Inorg. Chem. 45 (2006) 4910.
[20] A. Ghosh, J. Biol. Inorg. Chem. 11 (2006) 671.
[21] J. Conradie, T. Wondimagegn, A. Ghosh, J. Phys. Chem. B 112 (2008) 1053.
[22] J. Conradie, A. Ghosh, J. Phys. Chem. B 111 (2007) 12621.
[23] J. Conradie, A. Ghosh, J. Chem. Theory Comput. 3 (2007) 689.
[24] S. Zein, S.A. Borshch, P. Fleurat-Lessard, M.E. Casida, H. Chermette, J. Chem. Phys. 126 (2007) 014105.
[25] A. Fouqueau, S. Mer, M.E. Casida, L.M. Lawson Daku, A. Hauser, T. Mineva, F. Neese, J. Chem. Phys. 120 (2004) 9473.
[26] A. Fouqueau, M.E. Casida, L.M. Lawson Daku, A. Hauser, F. Neese, J. Chem. Phys. 122 (2005) 044110.
[27] L.M. Lawson Daku, A. Vargas, A. Hauser, A. Fouqueau, M.E. Casida, ChemPhysChem 6 (2005) 1393.
[28] X. Xu, W.A. Goddard III, Proc. Natl. Acad. Sci. USA 101 (2004) 2673.
[29] Y. Zhao, D.G. Truhlar, Theor. Chem. Acc. 120 (2008) 215.
[30] M. Swart, A.W. Ehlers, K. Lammertsma, Mol. Phys. 102 (2004) 2467.
[31] N.C. Handy, A.J. Cohen, Mol. Phys. 99 (2001) 403.
[32] J.P. Perdew, K. Burke, M. Ernzerhof, Phys. Rev. Lett. 77 (1996) 3865.
[33] J. Conradie, A. Ghosh, J. Chem. Theory Comput. 3 (2007) 689.
[34] Y.-Q. Zhang, C.-L. Luo, J. Phys. Chem. A 110 (2006) 5096.
[35] Y. Zhang, A. Wu, X. Xu, Y. Yan, Chem. Phys. Lett. 421 (2006) 383.
[36] A. Wu, Y. Zhang, X. Xu, Y. Yan, J. Comput. Chem. 28 (2007) 2431.
[37] M. Swart, Inorg. Chim. Acta 360 (2007) 179.
[38] A.R. Groenhof, A.W. Ehlers, K. Lammertsma, J. Am. Chem. Soc. 129 (2007) 6204.
[39] E. Derat, D. Kumar, R. Neumann, S. Shaik, Inorg. Chem. 45 (2006) 8655.
[40] S. Romo, J.A. Fernández, J.M. Maestre, B. Keita, L. Nadjo, C. de Graaf, J.M. Poblet, Inorg. Chem. 46 (2007) 4022.
[41] C. Rong, S. Lian, D. Yin, B. Shen, A. Zhong, L. Bartolotti, S. Liu, J. Chem. Phys. 125 (2006) 174102.
[42] M.-S. Liao, J.D. Watts, M.-J. Huang, J. Comput. Chem. 27 (2006) 1577.
[43] M.-S. Liao, J.D. Watts, M.-J. Huang, J. Phys. Chem. A 111 (2007) 5927.
[44] M. Swart, M. Güell, M. Solà, in: C.F. Matta (Ed.), Quantum Biochemistry: Electronic Structure and Biological Activity, Wiley, in press.

[45] C. Acosta-Silva, V. Branchadell, Results shown at DFT2007 Congress.
[46] M. Swart, M. Solà, F.M. Bickelhaupt, J. Comput. Chem. 28 (2007) 1551.
[47] M. Güell, J.M. Luis, M. Solà, M. Swart, J. Phys. Chem. A 112 (2008) 6384.
[48] D.L. Reger, Commun. Inorg. Chem. 21 (1999) 1.
[49] W. Hückel, H. Bretschneider, Ber. Deutsch. Chem. Ges. 70 (1937) 2024.
[50] D.L. Reger, T.C. Grattan, K.J. Brown, C.A. Little, J.J.S. Lamba, A.L. Rheingold, R.D. Sommer, J. Organomet. Chem. 607 (2000) 120.
[51] P. Gütlich, H. Goodwin, Spin Crossover in Transition Metal Compounds I–III, Springer-Verlag, Berlin, 2004.
[52] H.R. Bigmore, S.C. Lawrence, P. Mountford, C.S. Tredget, Dalton Trans. (2005) 635.
[53] C. Pettinari, R. Pettinari, Coord. Chem. Rev. 249 (2005) 525.
[54] D.L. Reger, C.A. Little, A.L. Rheingold, M. Lam, L.M. Liable-Sands, B. Rhagitan, T. Concolino, A. Mohan, G.J. Long, V. Briois, F. Grandjean, Inorg. Chem. 40 (2001) 1508.
[55] D.L. Reger, C.A. Little, V.G. Young, P. Maren, Inorg. Chem. 40 (2001) 2870.
[56] D.L. Reger, C.A. Little, M.D. Smith, A.L. Rheingold, K.C. Lam, T.L. Concolino, G.J. Long, R.P. Hermann, F. Grandjean, Eur. J. Inorg. Chem. (2002) 1190.
[57] C. Piquer, F. Grandjean, O. Mathon, S. Pascarelli, D.L. Reger, C.A. Little, G.J. Long, Inorg. Chem. 42 (2003) 982.
[58] D.L. Reger, J.D. Elgin, M.D. Smith, F. Grandjean, L. Rebbouh, G. Long, J. Eur. J. Inorg. Chem. (2004) 3345.
[59] D.L. Reger, J.R. Gardinier, J.D. Elgin, M.D. Smith, D. Hautot, G.J. Long, F. Grandjean, Inorg. Chem. 45 (2006) 8862.
[60] J.J. McGarvey, H. Toftlund, A.H.R. Alobaidi, K.P. Taylor, S.E.J. Bell, Inorg. Chem. 32 (1993) 2469.
[61] J.R. Sheets, F.A. Schultz, Polyhedron 23 (2004) 1037.
[62] E.J. Baerends, J. Autschbach, A. Bérces, J.A. Berger, F.M. Bickelhaupt, C. Bo, P.L. de Boeij, P.M. Boerrigter, L. Cavallo, D.P. Chong, L. Deng, R.M. Dickson, D.E. Ellis, M. van Faassen, L. Fan, T.H. Fischer, C. Fonseca Guerra, S.J.A. van Gisbergen, J.A. Groeneveld, O.V. Gritsenko, M. Grüning, F.E. Harris, P. van den Hoek, C.R. Jacob, H. Jacobsen, L. Jensen, E.S. Kadantsev, G. van Kessel, R. Klooster, F. Kootstra, E. van Lenthe, D.A. McCormack, A. Michalak, J. Neugebauer, V.P. Nicu, V.P. Osinga, S. Patchkovskii, P.H.T. Philipsen, D. Post, C.C. Pye, W. Ravenek, P. Romaniello, P. Ros, P.R.T. Schipper, G. Schreckenbach, J.G. Snijders, M. Solà, M. Swart, D. Swerhone, G. te Velde, P. Vernooijs, L. Versluis, l. Visscher, O. Visser, F. Wang, T.A. Wesolowski, E.M. van Wezenbeek, G. Wiesenekker, S.K. Wolff, T.K. Woo, A.L. Yakovlev, T. Ziegler, ADF 2007.01; SCM, Amsterdam, The Netherlands, 2007.
[63] M. Swart, F.M. Bickelhaupt, J. Comput. Chem. 29 (2008) 724.
[64] M. Swart, F.M. Bickelhaupt, Int. J. Quant. Chem. 106 (2006) 2536.
[65] G. te Velde, F.M. Bickelhaupt, E.J. Baerends, C. Fonseca Guerra, S.J.A. van Gisbergen, J.G. Snijders, T. Ziegler, J. Comput. Chem. 22 (2001) 931.
[66] F.M. Bickelhaupt, E.J. Baerends, Reviews in Computational Chemistry, vol. 15, Wiley-VCH, New York, 2000, p. 1.
[67] E.J. Baerends, V. Branchadell, M. Sodupe, Chem. Phys. Lett. 265 (1997) 481.
[68] W.G. Han, L. Noodleman, Inorg. Chem. 47 (2008) 2975.
[69] W.G. Han, T.Q. Liu, T. Lovell, L. Noodleman, J. Comput. Chem. 27 (2006) 1292.
[70] W.G. Han, L. Noodleman, Inorg. Chim. Acta 361 (2008) 973.
[71] H. Paulsen, A.X. Trautwein, J. Phys. Chem. Solids 65 (2004) 793.
[72] F. Remacle, F. Grandjean, G. Long, J. Inorg. Chem. 47 (2008) 4005.
[73] S. Trofimenko, J.C. Calabrese, P.J. Domaille, J.S. Thompson, Inorg. Chem. 28 (1989) 1091.
[74] J.C. Calabrese, P.J. Domaille, J.S. Thompson, S. Trofimenko, Inorg. Chem. 29 (1990) 4429.
[75] S. Calogero, G.G. Lobbia, P. Cecchi, G. Valle, J. Friedl, Polyhedron 13 (1994) 87.
[76] S. Zamponi, G. Gambini, P. Conti, G.G. Lobbia, R. Marassi, M. Berrettoni, P. Cecchi, Polyhedron 14 (1995) 1929.
[77] P. Cecchi, M. Berrettoni, M. Giorgetti, G.G. Lobbia, S. Calogero, L. Stievano, Inorg. Chim. Acta 318 (2001) 67.
[78] H. Paulsen, L. Duelund, A. Zimmermann, F. Averseng, M. Gerdan, H. Winkler, H. Toftlund, A.X. Trautwein, Monatsh. Chem. 134 (2003) 295.
[79] V. Briois, P. Sainctavit, G.J. Long, F. Grandjean, Inorg. Chem. 40 (2001) 912.
[80] C. Janiak, S. Temizdemir, S. Dechert, W. Deck, F. Girgsdies, J. Heinze, M.J. Kolm, T.G. Scharmann, O.M. Zipffel, Eur. J. Inorg. Chem. (2000) 1229.
[81] A.L. Rheingold, G. Yap, S. Trofimenko, Inorg. Chem. 34 (1995) 759.
[82] A.L. Rheingold, B.S. Haggerty, G.P.A. Yap, S. Trofimenko, Inorg. Chem. 36 (1997) 5097.
[83] J. Kruszewski, T.M. Krygowski, Tetrahedron Lett. 13 (1972) 3839.
[84] J. Tabernor, L.F. Jones, S.L. Heath, C. Muryn, G. Aromi, J. Ribas, E.K. Brechin, D. Collison, Dalton Trans. (2004) 975.
[85] N. Tsuchiya, A. Tsukamoto, T. Ohshita, T. Isobe, M. Senna, N. Yoshioka, H. Inoue, Solid State Sci. 3 (2001) 705.
[86] F. Grandjean, G.J. Long, B.B. Hutchinson, L. Ohlhausen, P. Neill, J.D. Holcomb, Inorg. Chem. 28 (1989) 4406.
[87] J.D. Oliver, D.F. Mullica, B.B. Hutchinson, W.O. Milligan, Inorg. Chem. 19 (1980) 165.
[88] G. Bruno, G. Centineo, E. Ciliberto, S. Dibella, I. Fragala, Inorg. Chem. 23 (1984) 1832.
[89] C. Janiak, T.G. Scharmann, J.C. Green, R.P.G. Parkin, M.J. Kolm, E. Riedel, W. Mickler, J. Elguero, R.M. Claramunt, D. Sanz, Chem.-Eur. J. 2 (1996) 992.
[90] G.J. Long, B.B. Hutchinson, Inorg. Chem. 26 (1987) 608.
[91] C. Hannay, M.J. HubinFranskin, F. Grandjean, V. Briois, J.P. Itie, A. Polian, S. Trofimenko, G.J. Long, Inorg. Chem. 36 (1997) 5580.
[92] G.G. Lobbia, B. Bovio, C. Santini, C. Pettinari, F. Marchetti, Polyhedron 16 (1997) 671.
[93] J.P. Jesson, J.F. Weiher, S. Trofimen, J. Chem. Phys. 48 (1968) 2058.
[94] F. Mani, Inorg. Nucl. Chem. Lett. 15 (1979) 297.
[95] P.A. Anderson, T. Astley, M.A. Hitchman, F.R. Keene, B. Moubaraki, K.S. Murray, B.W. Skelton, E.R.T. Tiekink, H. Toftlund, A.H. White, J. Chem. Soc., Dalton Trans. (2000) 3505.
[96] D.M. Eichhorn, W.H. Armstrong, Inorg. Chem. 29 (1990) 3607.
[97] J.C. Calabrese, P.J. Domaille, S. Trofimenko, G.J. Long, Inorg. Chem. 30 (1991) 2795.
[98] G.G. Lobbia, B. Bovio, C. Santini, P. Cecchi, C. Pettinari, F. Marchetti, Polyhedron 17 (1998) 17.
[99] J.P. Jesson, S. Trofimen, D.R. Eaton, J. Am. Chem. Soc. 89 (1967) 3158.
[100] A. Gulino, E. Ciliberto, S. Dibella, I. Fragala, Inorg. Chem. 32 (1993) 3759.
[101] S. Trofimenko, J. Am. Chem. Soc. 89 (1967) 3170.
[102] S. Trofimenko, J. Am. Chem. Soc. 89 (1967) 6288.
[103] C. Janiak, T.G. Scharmann, T. Brauniger, J. Holubova, M. Nadvornik, Z. Anorg. Allg. Chem. 624 (1998) 769.